Nuclear Materials and Energy 34 (2023) 101340

Contents lists available at ScienceDirect

Nuclear Materials and Energy

journal homepage: www.elsevier.com/locate/nme

First 3D modelling of tungsten erosion and migration in WEST discharges adopting a toroidally non-symmetric wall geometry

S. Di Genova [a,*], G. Ciraolo [b], A. Gallo [b], J. Romazanov [c], N. Fedorczak [b], H. Bufferand [b], P. Tamain [b], N. Rivals [b], Y. Marandet [d], S. Brezinsek [c], E. Serre [a], the WEST team [1]

[a] M2P2, Aix-Marseille Université, CNRS, Centrale Marseille, 13013 Marseille, France
[b] IRFM, CEA-Cadarache, 13108 Saint-Paul-lez-Durance, France
[c] IEK-4, Forschungszentrum Jülich, 52425 Jülich, Germany
[d] PIIM, Aix-Marseille Université, CNRS, 13013 Marseille, France

ARTICLE INFO

Keywords:
3D Boundary plasma modelling
Tungsten erosion and migration
WEST tokamak
Plasma-wall interaction
Toroidally localized limiters

ABSTRACT

Numerical analysis is a useful tool to investigate tungsten (W) sources and transport across plasma in W Environment Steady state Tokamak (WEST) plasma discharges, as it highlights physical mechanisms not always directly observable in experiments. Modelling activities were performed to study W erosion from WEST plasma-facing components (PFCs), as well as W migration through the plasma. For the first time, it was adopted a toroidally asymmetric wall geometry consisting of toroidally localized objects representing WEST antennas. To simulate WEST boundary plasma, 3D non-axisymmetric SOLEDGE transport simulations were performed with simplifying assumptions (pure deuterium plasma, a fluid model for neutrals). Results were then used as background for ERO2.0 runs to model W migration. On the sides of the toroidally localized objects, two thin stripes modelled WEST W antenna protections. Simulations suggest that particles eroded from the antennas protections may dominate the core W contamination in the analysed wall configuration. The findings suggest that these 3D non-axisymmetric models may be needed on a broader range of plasma conditions and wall configurations to accurately model the W migration in WEST.

1. Introduction

Studying erosion and migration of high Z elements in tokamaks is a necessary step to understand the physics in current devices so that next generation fusion experiments can be properly designed. Tungsten (W) is considered to be the most suitable plasma-facing component (PFC) material for future reactors. W has already been widely tested in tokamaks such as ASDEX Upgrade [1] and JET-ILW [2]. Some of the Tungsten Environment Steady state Tokamak (WEST) [3] main goals are to study the feasibility of using W in steady operations, being a long pulse operation machine, and to test the divertor monoblocks that will be employed for ITER. WEST operations are largely influenced by W erosion and migration into the confined plasma, as W represents the bulk material of the divertor monoblocks and it is the coating material for all of the PFCs. Some of the WEST PFCs are toroidally localized objects, as shown in Fig. 1(a). These objects are usually located close to the hot confined plasma, and they act as limiters. WEST limiters in plasma discharges start-up, or the radio frequency (RF) antenna protections during plasma discharges, are severely eroded [4] and suspected to have a predominant impact in influencing WEST core W content.

In previous contributions, numerical modelling was performed to study W erosion and migration at WEST PFCs [5–7] under the assumption of axisymmetric wall geometry. In this work, we introduce for the first time numerical analyses of W erosion and migration in WEST using 3D simulations with an asymmetric wall geometry composed of both axisymmetric PFCs and toroidally localized objects, as shown in Fig. 1(b).

The next section of the document is focused on the description of the wall geometry. It follows the set-up for SOLEDGE [8] and ERO2.0 [9] simulations, together with the discussion of the results.

2. Wall geometry model

The wall model was modified from the previous axisymmetric version. The former axisymmetric wall had a single wide toroidal outer limiter (i.e. an axisymmetric toroidal ring) as shown in Fig. 2. The

* Corresponding author.
E-mail address: stefano.di-genova@univ-amu.fr (S. Di Genova).
[1] http://irfm.cea.fr/en/west/WESTteam/.

https://doi.org/10.1016/j.nme.2022.101340
Received 29 June 2022; Received in revised form 28 November 2022; Accepted 11 December 2022
Available online 12 December 2022

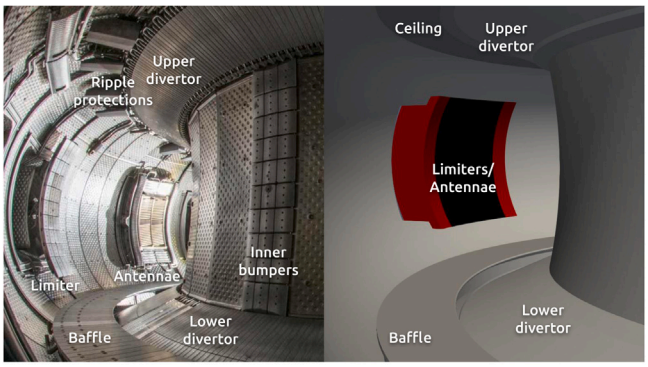

Fig. 1. (a) WEST PFCs, completely made by bulk W, or coated with W (up to C4 campaign, 2019). Inner bumpers, RF antennas, and the outboard limiter are toroidally localized objects. (b) New simplified WEST wall model, composed of axisymmetric surfaces and toroidally localized PFCs.

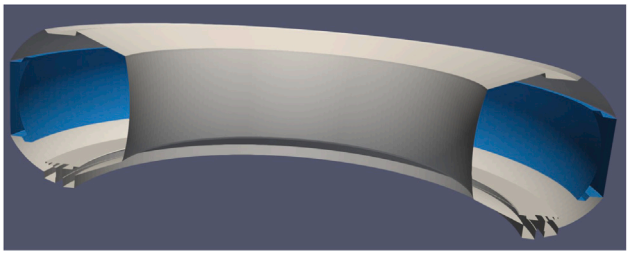

Fig. 2. Previous WEST axisymmetric wall model adopted in [5,6]. The axisymmetric limiter being the blue component. (For interpretation of the references to colour in this figure legend, the reader is referred to the web version of this article.)

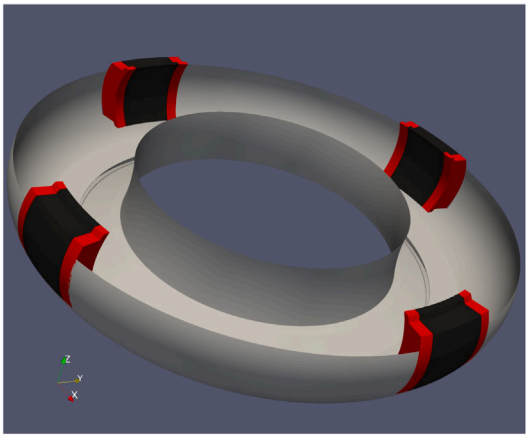

Fig. 3. New WEST asymmetric wall model, including toroidally localized PFCs. Grey (axisymmetric) PFCs were always considered W sources, black PFCs were never considered W sources. Red PFCs (antenna protections) W erosion was switched on and off to study its impact on W confined plasma contain. (For interpretation of the references to colour in this figure legend, the reader is referred to the web version of this article.)

axisymmetric limiter surface was much larger than the area wet by the plasma of antennas and the limiter in WEST experiments. Hence, the outboard limiter was retracted by a distance of roughly 20 cm to avoid overestimating plasma recycling and W erosion [5]. This distance was not chosen with any particular criteria, and it was way larger than the usual WEST distances between the confined plasma and the closer PFCs. For instance, the antennas have a distance from the separatrix between 1 cm and 6 cm when RF power is injected [4]. Due to the artificially increased distance to the main separatrix, the limiter contribution to the overall core W content was often negligible in simulations [6]. This underlines the intricacy of studying the effects of WEST outboard limiter and antennas using 2D axisymmetric simulations.

Improving the accuracy of the wall geometry in the simulations by using a new non-axisymmetric wall geometry with toroidally localized objects (see Fig. 3) was possible thanks to new SOLEDGE developments allowing for 3D resolved simulations [10]. The new wall was consists of four toroidally localized antennas. The four antennas were located 90° apart, with their distance from the separatrix of the considered magnetic configuration being about 1.5 cm. In WEST experiments, the distance between separatrix and the first object in the Low Field Side (LFS) is on average roughly 3 cm, but values between 1 cm and 2 cm are not excluded [4], so the distance considered here can be seen as a lower limit.

The wall PFCs were classified into three different types as shown in Fig. 3: The Axisymmetric ones (grey objects) were always considered W sources. The ones consisting of the body of the antennas (black objects, 10° wide) were never considered W sources, as they were aimed to represent the antennas central components, which are made of middle Z elements such as silver (Ag) and copper (Cu). Finally, the ones consisting of the sides of antennas (red objects, 3.5° wide) were not considered W sources in a first simulation and then used as W sources in a second run to study their impact on the overall W core content. The purpose of those PFCs was to model W antennas protections present in WEST. All components were considered as possible W deposition areas. No W self-erosion of these components was considered.

Due to technological limitations that will be discussed in the next section, in this model the wall surface was either parallel or orthogonal to the toroidal direction. Thus, the PFCs were intersected by the toroidal magnetic field with an azimuthal angle that could be either 0°, as the axisymmetric components, or 90°, as the side surfaces of the antennas. However, the presence of the poloidal magnetic field prevented a null intersection between the field and the wall. Due to this limitation, the exact geometric shape of the antenna protections could not be resolved in these simulations, and the magnetic field intersected the sides of the antenna protections nearly orthogonally.

3. Boundary plasma modelling

Boundary plasma was modelled by SOLEDGE [8,10]. SOLEDGE is a fluid code solving mass, momentum, and energy conservation equations for multiple species from the edge plasma up to the first wall in complex geometries. SOLEDGE adopts a flux-surface aligned structured mesh in which quadrangles in the poloidal plane are extruded in the toroidal direction. The wall geometry is imposed through mesh immersed boundary conditions. As a consequence, the wall surfaces cannot be tilted with respect to the toroidal direction as mentioned in the previous section.

The simulation here described was in pure deuterium (D), turbulent phenomena were accounted only on “large” tokamak scales through diffusive processes (i.e. a transport simulation). The mean-field transport coefficients for particle cross-field diffusion $D_\perp$ and viscosity $\nu_\perp$ were such that $D_\perp = \nu_\perp = 0.3$ m^2/s, and cross-field heat conductivity for ions $\chi_\perp^i$ and electrons $\chi_\perp^e$ were such that $\chi_\perp^i = \chi_\perp^e = 1$ m^2/s. Drifts were not included in the runs. The coupling between SOLEDGE and EIRENE, accomplished in 2D simulations [8], is still in development for 3D simulations at the time of writing of this work. Thus, neutral physics was handled with a diffusive model in SOLEDGDE itself.

The total power entering the scrape-off layer P_{SOL} was set to 1 MW, the electron density n_e at the core-edge interface (the simulation inner boundary) was set to 5×10^{19} m^{-3}. A neutral deuterium gas injection rate (or puff) of 7×10^{20} s^{-1} was located in the private flux region, and the recycling coefficient was set equal to 97% on the whole wall surface. Hence, 3% of the flux was not recycled to mimic neutral pumping effects with a simple proxy. The simulation domain was

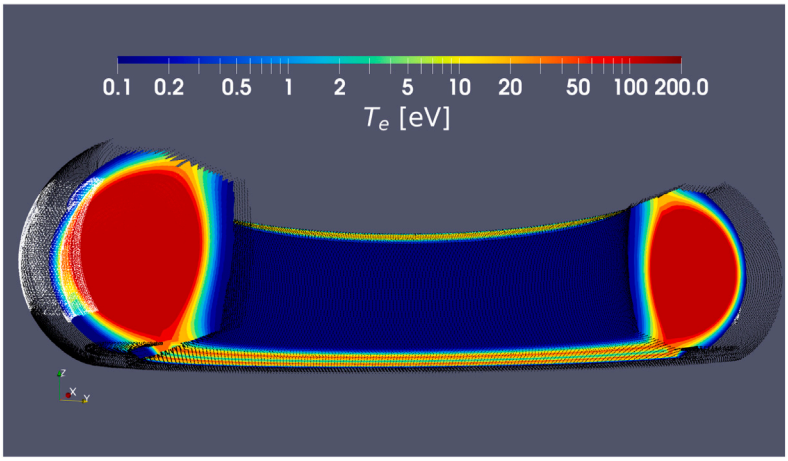

Fig. 4. T_e iso-surfaces on half of a torus, including only the surfaces with $T_e > 0.1$ [eV]. Black dots represent the axisymmetric part of the wall, white dots represent the antennas.

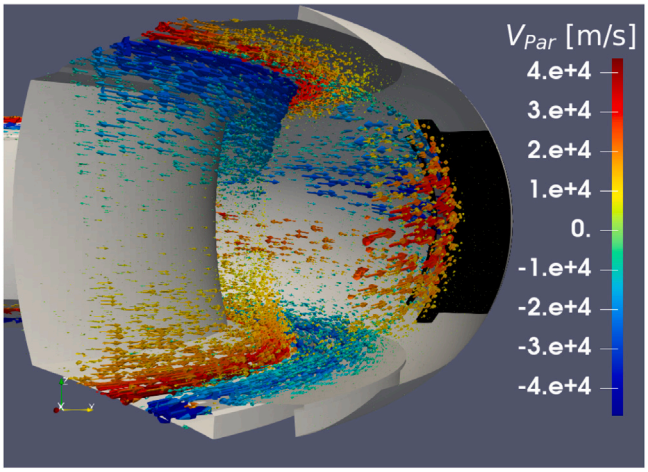

Fig. 5. Plasma parallel velocity field, shown from a torus poloidal cross-section. The magnetic field enters in the figure plane, going in counterclockwise direction seeing the tokamak from the top. Red arrows go in the same direction of the magnetic field, blue arrows go in the counter direction. (For interpretation of the references to colour in this figure legend, the reader is referred to the web version of this article.)

symmetric with respect to a quarter of a torus. The quarter of torus toroidal discretization consisted of 32 sectors of roughly 0.05 rad each (2.81°).

Representative figures of the 3D simulation can be found in Figs. 4 and 5. Fig. 5 represents the parallel velocity field $v_\parallel$ in a poloidal cross-section of the torus. At the LFS, plasma flow is axisymmetric in the magnetic field direction at the top of the machine, and flows in the opposite direction at the bottom. The presence of toroidally localized objects breaks the axisymmetry, with plasma flowing in opposite directions at the two sides of the antenna. Despite the simplified model, SOLEDGE results were consistent with the parameters inside WEST operational space in L-mode [6,11,12]. Figs. 6 and 7 show electron density n_e and temperature T_e at the outer midplane and divertor targets respectively in the simulation, at a toroidal angle halfway between two antennas. n_e at the outer midplane separatrix was 2.5×10^{19} [m^{-3}], going up to 3.4×10^{19} [m^{-3}] at the outer target due to recycling at divertor plates. T_e went from 50 [eV] at the separatrix down to 30 [eV] at the outer target, indicating that the plasma was in conduction limited regime. In Fig. 8 it is shown the plasma parallel velocity field at a radial location beyond the surface of the antennas: The field lines connect 2 antennas. Therefore, to satisfy the Bohm boundary condition at both ends of the field line, a parallel flow stagnation point is located at

Table 1
Average and maximum values assumed by physical quantities along the toroidal angle φ at the midplane at antenna surface radial location.

	$<>_{2\pi}$	$\text{Max}()_{2\pi}$
T_e [eV]	31.4	31.8
T_i [eV]	55.2	55.8
n_e [10^{18} m^{-3}]	6.0	7.0
$v_\parallel$ [10^4 m s^{-1}]	0.2	2.0

Table 2
Erosion rate and confined plasma contamination computed by ERO2.0. The Antenna protections contribute 90% of the overall W content inside the separatrix, but 85% of the erosion comes from the rest of the PFCs.

	Antenna protection	Rest of PFCs
Erosion rate [s^{-1}]	3.27×10^{19}	2.54×10^{20}
W ions inside separatrix [/]	9.00×10^{16}	9.95×10^{15}

the halfway point between the two antennas. In Fig. 9 the relative midplane toroidal modulation at radial location of antennas surface is shown for n_e, T_e, the ion temperature T_i, and $v_\parallel$. The relative midplane toroidal modulation of a quantity A at a given toroidal angle value φ is defined as $\bar{A}(\varphi) = (A(\varphi) - \langle A \rangle_{2\pi})/\text{Max}(A)_{2\pi}$, where $\langle \cdots \rangle_{2\pi}$ is the toroidal average and $\text{Max}(\ldots)_{2\pi}$ is the maximum on the toroidal angle. These values are reported for each physical quantity in Table 1: T_i at antennas major radius was roughly 50 [eV] and its variation along the toroidal angle was negligible, likewise, T_e modulation in the toroidal direction was also insignificant, as visible in Fig. 4. On the other hand, $v_\parallel$ strongly varied along the toroidal field, as plasma went repeatedly from stagnant to sound speed along the magnetic lines as a result of the Bohm condition at the antennas surfaces, as can be seen in Fig. 8. n_e slightly varied along the toroidal direction as a consequence of the plasma flow accelerating and the plasma recycling at the antennas surface.

4. W erosion and migration modelling

W erosion and migration were modelled with ERO2.0 [9]. ERO2.0 is a code for Monte Carlo impurity tracking and surface erosion and deposition simulation. SOLEDGE results described in Section 3 were used as plasma background for ERO2.0 runs, with SOLEDGE and ERO2.0 simulation wall geometries being identical. Applying interpolation, ERO2.0 would be capable of handling any wall geometry, regardless of the one used for the plasma background. However, in these results both SOLEDGE and ERO2.0 used the same wall geometry in order to maintain consistency.

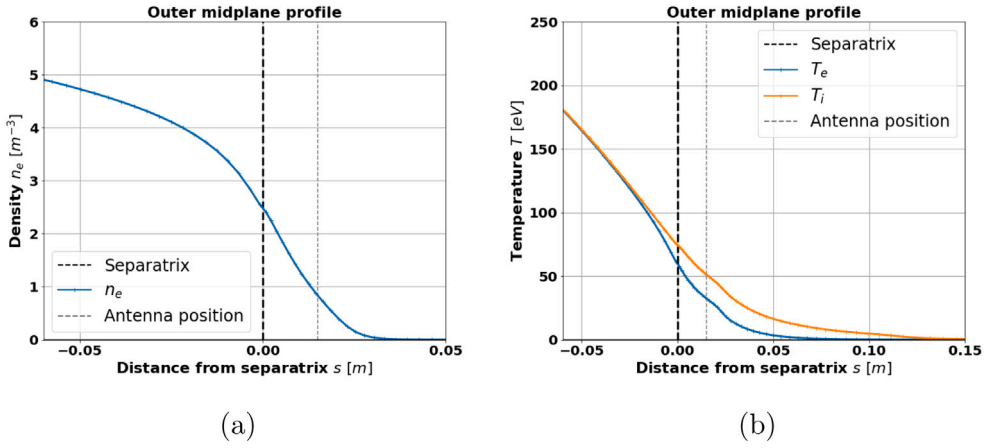

Fig. 6. SOLEDGE results at the outer midplane for a toroidal angle equidistant from two consecutive antennas, showing: (a) n_e, and (b) T_i and T_e.

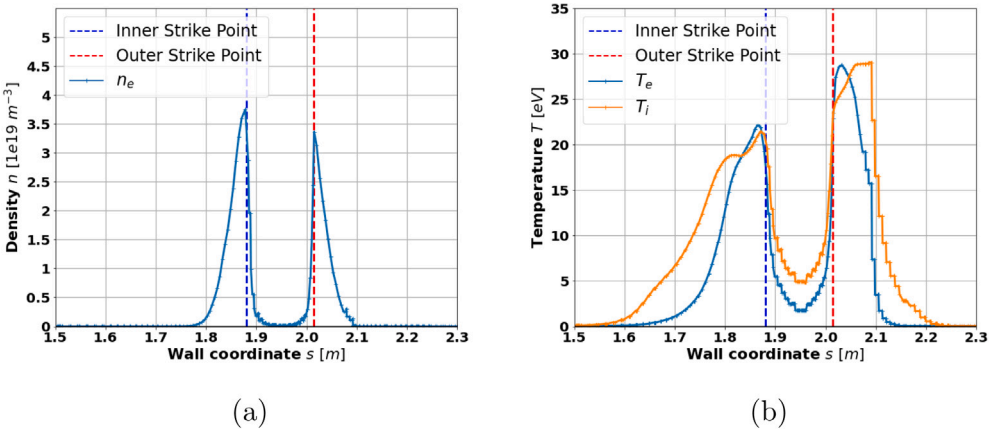

Fig. 7. SOLEDGE results at divertor targets for a toroidal angle equidistant from two consecutive antennas showing: (a) n_e, and (b) T_i and T_e.

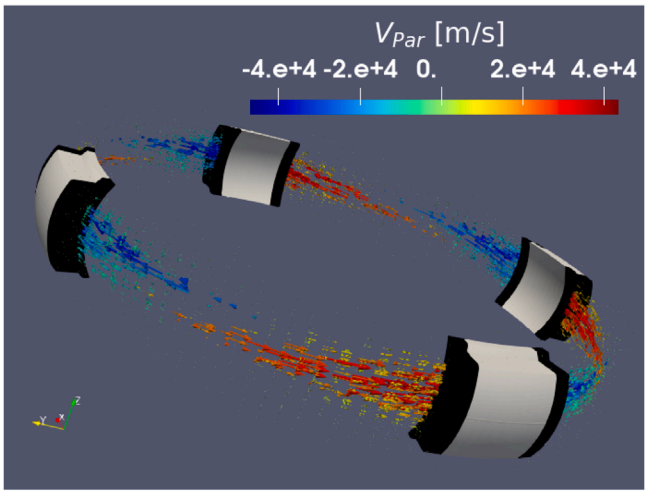

Fig. 8. Plasma parallel velocity field beyond the antennas surface radial location.

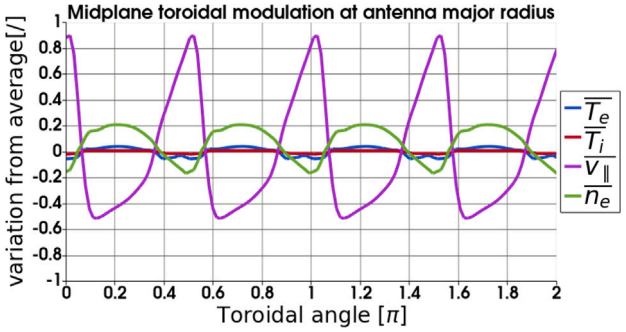

Fig. 9. Relative midplane toroidal modulation of plasma physical quantities as defined in Section 3. T_i and T_e vary from the average along the toroidal direction for less than 5% of the maximum assumed value. The modulations are more significant for n_e and $v_\parallel$.

W sputtered by D is negligible compared to sputtering by light impurities in L-mode discharges [13]. Thus, uniform concentration values of oxygen (O) of 3% were set in ERO2.0 simulations as a proxy of the different light impurities usually found in WEST such as nitrogen (N), boron (B), and carbon (C) [14]. The abundance (i.e. relative concentration) of O ionization states from 1+ to 8+ was set to be equal to the values found at the WEST divertor of 2D SOLEDGE simulations in which the O distribution was computed self-consistently and compared to experimental data [11]. Thompson distribution [15] was used for the energy of the sputtered particles, while a butterfly-like distribution [15] was used for the azimuthal angle of sputtered W. Turbulent transport was modelled with random cross-field displacements equal to $\sqrt{4D_\perp \Delta t}$, where Δt is the particles time-step, and $D_\perp$ is the diffusion coefficient. $D_\perp$ was set equal to the value used in SOLEDGE. Inside the sheath, the electrostatic potential ϕ followed the Borodkina model [16]. The Borodkina model is a simplified version of the Chodura model [17] that allows for computing ϕ distribution without solving integral equations.

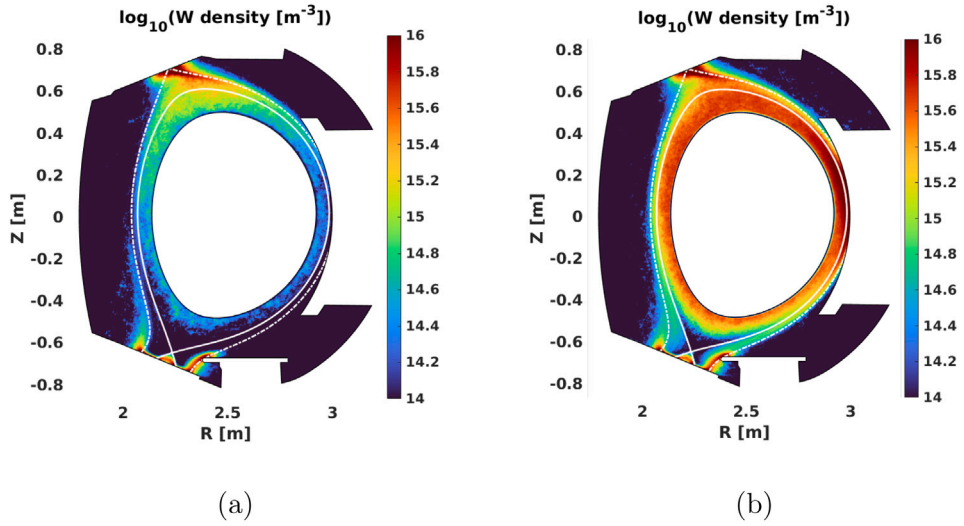

Fig. 10. W density maps: (a) without considering antenna protections W erosion, and (b) considering it.

n_e dropped proportionally to the Boltzmann factor $\exp(e\phi/T_e)$ [18], where e is the electron charge. Collisional forces consisted of the kinetic formulation for both friction forces F_0 and thermal forces $F_{\nabla T}$ of the plasma background ions on the sputtered particles as described in literature [19,20]. Contamination from W self-sputtering was not included to keep the analyses simple and linear. Outside the sheath, the electric force was neglected, as it is typically smaller than collisional forces for impurities. In fact, the electric force is proportional to the particles charge, whereas collisional forces are proportional to the square of the charge [18]. $\vec{B} \times \nabla B$ drifts were self-consistently computed from the Lorentz force, as well as $\vec{E} \times \vec{B}$ inside the sheath.

As explained in Section 2, simulations were runs with and without W erosion at antenna protections. Fig. 10 shows W density maps from the two cases results: in the case without the antenna protections erosion, the upper divertor contributed the most to W content inside the confined plasma. While in the second case W coming from the antenna protections dominates the contamination of the core. The global picture of the density map changes between the two cases, with the edge W level being roughly one order of magnitude higher in the case including the antenna protections erosion. As self-sputtering was not included in the simulations, the global effect of the erosion of all the PFCs on the overall W core content was the superposition of the effects of the erosion of the single PFCs. Therefore, the difference in W density between simulations is purely caused by the erosion of the antenna protections. Table 2 reports the values of the total number of W particles found inside the separatrix coming from the antenna protections and the rest of the PFCs. Likewise, the erosion rates of the two groups of PFCs are also written in the table. Plasma interaction with the axisymmetric PFCs (lower divertor, upper divertor, baffle, tokamak ceiling) causes 85% of the erosion rate, but 90% of W particles found in the separatrix comes from the antenna protection. This result may overestimate the actual impact of the antenna protection in experiments, as the distance from the separatrix is a lower limit. Nevertheless, the impact of the toroidally localized objects seems to be significant. This is in qualitative agreement with what observed experimentally on other full-W devices [1].

5. Conclusions

WEST boundary plasma, wall erosion, and W migration were modelled in a toroidally asymmetric wall geometry by including toroidally localized objects. SOLEDGE 3D simulations were carried out to reproduce plasma main species (D and e) conditions, using a simple fluid model for neutrals and diffusive processes as a proxy for turbulent transport. ERO2.0 simulations were run to model W erosion and migration, adopting a 3% O uniform concentration to account for W sputtering by light impurities. Simulations were repeated with and without accounting for W erosion at antenna protections. The impact of the antenna protections on the overall W content inside the separatrix in the considered configuration suggests that taking into account toroidally localized objects may be necessary to accurately simulate boundary phenomena and impurity physics in WEST discharges. Results encourage further modelling adopting 3D toroidally asymmetric walls, scanning antennas distance from the separatrix, and analysing different plasma regimes and scenarios.

CRediT authorship contribution statement

S. Di Genova: Numerical modelling, Data processing, Results analysis, Data visualization, Manuscript writing. **G. Ciraolo:** Numerical modelling, Modelling discussion, Project management. **A. Gallo:** Results analysis, Physics discussion, Project management, Manuscript revision. **J. Romazanov:** Code developer, Modelling discussion, Physics discussion, Manuscript revision. **N. Fedorczak:** Results analysis, Physics discussion. **H. Bufferand:** Code developing, Data processing. **P. Tamain:** Code developing, Manuscript revision. **N. Rivals:** Code developing. **Y. Marandet:** Project management, Manuscript revision. **S. Brezinsek:** Project management. **E. Serre:** Project management, Manuscript revision. **the WEST team:** Data management.

Declaration of competing interest

The authors declare that they have no known competing financial interests or personal relationships that could have appeared to influence the work reported in this paper.

Data availability

Data will be made available on request.

Acknowledgements

This work has been carried out within the framework of the EUROfusion Consortium, funded by the European Union via the Euratom Research and Training Programme (Grant Agreement No 101052200 - EUROfusion). Views and opinions expressed are however those of the author(s) only and do not necessarily reflect those of the European Union or the European Commission. Neither the European Union nor the European Commission can be held responsible for them.

References

[1] A. Kallenbach, et al., Non-boronized compared with boronized operation of ASDEX upgrade with full-tungsten plasma facing components, Nucl. Fusion 49 (4) (2009) 045007.

[2] S. Brezinsek, et al., Plasma-surface interaction in the Be/W/ environment: Conclusions drawn from the JET-ILW for ITER, J. Nucl. Mater. 463 (2015) 11–21, PLASMA-SURFACE INTERACTIONS 21.

[3] J. Bucalossi, et al., The WEST project: Testing ITER divertor high heat flux component technology in a steady state tokamak environment, Fusion Eng. Des. 89 (7) (2014) 907–912, Proceedings of the 11th International Symposium on Fusion Nuclear Technology-11 (ISFNT-11) Barcelona, Spain, 15-20 September, 2013.

[4] G. Urbanczyk, et al., RF wave coupling, plasma heating and characterization of induced plasma-material interactions in WEST L-mode discharges, Nucl. Fusion 61 (2021).

[5] A. Gallo, et al., First efforts in numerical modeling of tungsten migration in WEST with SolEdge2D-EIRENE and ERO2.0, Phys. Scr. T171 (2020).

[6] S.D. Genova, et al., Modelling of tungsten contamination and screening in WEST plasma discharges, Nucl. Fusion 61 (10) (2021).

[7] Y. Marandet, et al., Assessment of tungsten sources in the edge plasma of WEST, J. Nucl. Mater. 463 (2015) 629–633, PLASMA-SURFACE INTERACTIONS 21.

[8] H. Bufferand, et al., Numerical modelling for divertor design of the WEST device with a focus on plasma–wall interactions, Nucl. Fusion 55 (5) (2015) 053025.

[9] J. Romazanov, et al., Beryllium global erosion and deposition at JET-ILW simulated with ERO2.0, Nucl. Mater. Energy 18 (2019) 331–338.

[10] H. Bufferand, et al., Three-dimensional modelling of edge multi-component plasma taking into account realistic wall geometry, Nucl. Mater. Energy 18 (2019) 82–86.

[11] A. Gallo, et al., Interpretative transport modeling of the WEST boundary plasma: main plasma and light impurities, Nucl. Fusion 60 (12) (2020).

[12] G. Ciraolo, et al., First modeling of strongly radiating WEST plasmas with SOLEDGE-EIRENE, Nucl. Mater. Energy 20 (2019) 100685.

[13] A. Huber, et al., Understanding tungsten erosion during inter/intra-ELM periods in he-dominated JET-ILW plasmas, Phys. Scr. 96 (12) (2021).

[14] G.J. van Rooij, et al., Tungsten divertor sources in WEST related to impurity inventory and local plasma conditions, Phys. Scr. T171 (2020) 014060.

[15] A. Eksaeva, et al., ERO modelling of tungsten erosion in the linear plasma device PSI-2, Nucl. Mater. Energy 12 (2017).

[16] I. Borodkina, et al., Surface biasing influence on the physical sputtering in fusion devices, in: Journal of Physics: Conference Series, Vol. 748, IOP Publishing, 2016, 012002.

[17] R. Chodura, Physics of Plasma-Wall Interactions in Controlled Fusion, Springer, New York, NY, 1986, p. 99.

[18] P.C. Stangeby, The Plasma Boundary of Magnetic Fusion Devices, in: Series in Plasma Physics and Fluid Dynamics, Taylor & Francis, 2000.

[19] D. Reiser, et al., Improved kinetic test particle model for impurity transport in tokamaks, Nucl. Fusion 38 (2) (1998) 165.

[20] Y. Homma, et al., Numerical modeling of thermal force in a plasma for test-ion transport simulation based on Monte Carlo binary collision model, J. Comput. Phys. 231 (8) (2012) 3211–3227.